

promoting access to White Rose research papers



Universities of Leeds, Sheffield and York
<http://eprints.whiterose.ac.uk/>

This is an author produced version of a paper published in ***Journal of Vibration and Acoustics***,

White Rose Research Online URL for this paper:
<http://eprints.whiterose.ac.uk/9272>

Published paper

Sims, N.D. Limit cycle behavior of smart fluid dampers under closed loop control. *Journal of Vibration and Acoustics, Transactions of the ASME*, 2006, **128**(4), 413-428.

<http://dx.doi.org/10.1115/1.2212444>

Limit Cycle Behaviour of Smart Fluid Dampers under Closed Loop Control

Neil D Sims

Department of Mechanical Engineering, The University of Sheffield,

Mappin St, Sheffield S1 3JD, UK

Email: n.sims@sheffield.ac.uk

Phone: +44 114 2227724

Fax: +44 114 2227890

35 pages including 12 Figures.

Abstract

Semi-active vibration dampers offer an attractive compromise between the simplicity and fail-safety of passive-devices, and the weight, cost and complexity of fully active systems. In addition, the dissipative nature of semi-active dampers ensures they always remain stable under closed loop control, unlike their fully-active counterparts. However, undesirable limit cycle behaviour remains a possibility which is not always properly considered during the controller design.

Smart fluids provide an elegant means to produce semi-active damping, since their resistance to flow can be directly controlled by the application of an electric or magnetic field. However, the nonlinear behaviour of smart fluid dampers makes it difficult to design effective controllers, and so a wide variety of control strategies has been proposed in the literature. In general this work has overlooked the possibility of undesirable limit cycle behaviour under closed loop conditions.

The aim of the present study is to demonstrate how the experimentally observed limit cycle behaviour of smart dampers can be predicted and explained by appropriate nonlinear models. The study is based upon a previously developed feedback control strategy, but the techniques described are relevant to other forms of smart damper control.

Introduction

It is well known that active damping can offer superior vibration control compared to traditional passive damping solutions. However, it is also accepted that active damping suffers high power requirements and has the potential to become unstable, making it unsuitable for many practical applications. As a result, semi-active damping has been heralded as offering a compromise between the performance capabilities of active systems and the simplicity and fail-safety of passive dampers. Whilst its energy dissipating nature means that unstable behaviour is impossible, semi-active damping can still exhibit undesirable limit cycle behaviour, and this has been largely overlooked in the literature.

One form of semi-active device that has received a great deal of interest in recent years is the so-called smart fluid damper. Here, a magneto-rheological (MR) or electro-rheological (ER) fluid is controlled by an applied magnetic or electric field, which changes the resistance to flow of the fluid and hence controls the damping behaviour of the device. Previous studies have developed smart fluid dampers for a variety of applications, including vehicle suspension systems [1], seismic control of structures [2], and vibration isolation problems [3]. A number of commercial applications have recently appeared, particularly in the automotive sector [4]. However, the nonlinear behaviour of smart fluid dampers has resulted in a wide variety of control strategies being proposed.

A number of researchers have used neural network controllers [5, 6] to overcome the nonlinear behaviour, with the advantage that no model of the device behaviour is required. However, the neural network requires training and its 'black box' nature may be unappealing to end users. Furthermore, the constitutive behaviour of smart dampers is now fairly well understood (see, for example, [7]) and so it seems sensible to harness this understanding to improve the controller's performance. One such approach is to use gain scheduling methods [8] to accommodate the nonlinearity, but the performance can then be susceptible to unexpected changes in the device behaviour, due (for example) to temperature variations. Other work has employed sliding mode control [9-11] to tackle the uncertainties and parameter variations of the system, or used H-infinity [12] and optimal [13] controllers. A far more straightforward approach is to implement on/off control strategies [1], but these fail to capitalise on the controllability offered by the smart damper.

Previous work by the author and his colleagues at Sheffield University has pursued an alternative approach based upon feedback linearisation. The aim here was to first linearise the behaviour of the damper so that it can be thought of as a semi-active force generator. This allows a wide range of classical or modern control techniques to be designed when incorporating the device into a vibrating structure, without having to consider the nonlinearity of the damping device. The approach was originally applied to an electrorheological damper [14] operating under sinusoidal mechanical excitation. It was shown that by making the reference force, or controller input signal, proportional to damper velocity, the device could be made to emulate a viscous damper with a controllable damping coefficient. During this work it was discovered [15] that under certain control conditions the response of the device became oscillatory in a fashion similar to limit cycle behaviour.

There has been some work to investigate the robustness of smart damper controllers [16], but in general previous work has offered little or no insight into the stability of the system. One exception is the work by Shukla and his colleague [17] which considered the nonlinear dynamics of a 2 degree-of-freedom structure, with an MR damper under proportional-derivative control. However, there was no experimental evidence to support the analysis.

In this article, the limit cycle behaviour of an MR damper under feedback control is analysed in detail using a previously validated model [7] and comprehensive experimental data. The article begins with a description of the experimental apparatus used for testing the MR damper, and some preliminary results are shown which illustrate the limit cycle behaviour. The model which will be used to explain this behaviour is then summarised for the sake of completeness. Next, the feedback control strategy is described and a stability analysis is performed on the resulting closed loop model. This starts with a linear stability analysis which is physically significant, but then moves on to investigate the nonlinear stability using a phase-space representation of the system dynamics, which is investigated numerically. Next, the results of the stability analyses are compared to comprehensive experimental data. Corresponding numerical simulations are used to illustrate the closed loop dynamics in phase-space. Finally, some conclusions are drawn.

Experimental setup

The damper used in this study was a commercially available device manufactured by Lord Corporation [18], and it was tested in a long-stroke damper test facility at The University of Sheffield. The test facility comprised an electric motor, gearbox, flywheel, and crank arrangement which mechanically excited the damper as shown in Figure 1a. The excitation frequency could be varied up to 15Hz and the excitation amplitude could be varied up to $\pm 8\text{mm}$. The MR damper was attached to the crank connecting rod with an intermediate rod and bearing assembly to produce linear motion, as shown in Figure 1b. The relative displacement across the damper was monitored with a Linear Variable Differential Transformer (LVDT) and the force measured with a load cell (both shown on Figure 1b). A dSPACE digital control system was used to acquire the experimental measurements and perform closed loop control. The controller used a sample frequency of 10kHz, although this was down-sampled to 1kHz for data storage purposes.

The controller design will be introduced later, but the basic aim was to make the device perform as a controllable viscous damper, using the damping force (measured via the LVDT) as a sensor signal. The controller input was the mechanical excitation velocity. In practical applications this could be measured using an electromagnetic velocity sensor, or by differentiating the LVDT signal as described in [14]. However, for the purposes of a stability analysis it is desirable to minimise any effect measurement noise might have on the closed loop dynamics of the system. For this reason, the velocity was generated artificially by the controller, since the mechanical excitation is essentially sinusoidal. A keyway and proximity probe on the end of the crank unit (shown in Figure 1b) were used to determine the excitation frequency and to synchronise the artificially generated velocity signal with the actual mechanical excitation.

In Figure 2, some typical results are shown from the apparatus under closed loop conditions. With appropriate choice of controller gains, the device can be made to behave as a controllable damper, as shown in Figure 2a. However, inappropriate choice of controller gains results in the undesirable behaviour shown in Figure 2b. Both these results demonstrate similar behaviour to the ER damper tested previously [15]. The remainder of this article is devoted to explaining the undesirable behaviour observed in Figure 2b.

Theory

MR damper model

The model that has been used in this study has been comprehensively described in a recent journal article [7]. Since the model forms a central aspect of the present study, it will be summarised below. For a more comprehensive description of the modelling and model updating approach, the reader is referred to reference [7].

The model is shown in lumped parameter form in Figure 3. Here, the spring k represents the compressibility of the fluid in the cylinder of the damper (due to the fluid bulk modulus and any entrapped air bubbles). This compressibility term has been shown to accurately account for the hysteresis loop that is observed in the force-velocity characteristic of smart dampers [7, 19]. The mass m_l in the model represents the inertia of the fluid as it flows through the valve within the damper. The flow through the valve is represented by nonlinear damper χ which is a function of the velocity \dot{x}_1 and the current, I :

$$\chi(\dot{x}_1, I) = \begin{cases} c_{pre}\dot{x}_1 & |\dot{x}_1| < \frac{F_y}{c_{pre} - c_{post}} \\ (c_{post}|\dot{x}_1| + F_y)\text{sgn}(\dot{x}_1) & |\dot{x}_1| \geq \frac{F_y}{c_{pre} - c_{post}} \end{cases} \quad (1)$$

Here, F_y is the yield force of the damper, which increases with applied current I . The variable c_{pre} represents the viscous damping in the so-called ‘pre-yield’ condition of the damper, and c_{post} is the viscous damping in the ‘post-yield’ condition. The values for these three variables were found empirically [7] and are given in Table 1.

With reference to Figure 3, a further complication arises due to the dynamics of the fluid excitation system. This system is comprised of a power amplifier and electromagnetic circuit, which generates a magnetic field that produces a change in yield stress of the MR fluid within the valve. The dynamics of this system are approximated by a 1st order lag term with a time constant τ . The input to the system is the so-called ‘control current’ I_C , and the output is the variable I as shown in Figure 3. The equations of motion for the system shown in Figure 3 are therefore:

$$\begin{aligned}
\dot{I} &= \frac{I_C - I}{\tau} \\
m_1 \ddot{x}_1 &= -\chi(\dot{x}_1, I) + k(x_2 - x_1) \\
F &= k(x_2 - x_1)
\end{aligned} \tag{2}$$

where the output F is the force generated by the MR damper in response to the input x_2 , as shown in Figure 3. Two points are worthy of note at this stage:

- Alternative formulations of smart valve flow have been described (e.g. Bingham plastic behaviour [20, 21] and Eyring behaviour [22]), which could be used in a similar fashion, by redefining the damping function χ (Equation (1)).
- The lumped parameter model presented in Figure 3 is analogous to a hydraulic power model representing fluid flow, fluid compliance, and fluid inertia [23].

In reference [7] the model described above was compared to experimental behaviour under broadband mechanical excitation in the range 0 to 20 Hz. Excellent agreement between model and experiment was observed, and a typical example of the model's performance is shown in Figure 4. Consequently the model can be used with confidence to explore the closed loop behaviour of the damper.

Closed loop model

The idea of linearising a smart damper's response using feedback control was first proposed in 1997 [24], in a numerical study, and was later implemented experimentally [14, 15]. In the present study, similar results have been obtained for the MR damper, as shown in Figure 2. The technique has also recently been shown to be effective under broadband mechanical excitation [25].

The underlying concept of the approach is to consider the MR damper as a control system with two inputs (current and velocity) and one output (damping force). The velocity is then treated as a disturbance input, which is perhaps counter-intuitive for a damping device. Next, proportional feedback control is applied to the controlled input as shown in Figure 5a. This approach was shown by West [26] to linearise the relationship between the input and output variables. Consequently the damper can now be thought of as a semi-active force generator. Provided the desired force F_R lies within the control limits of the device, the damper control signal will be automatically tuned to achieve a corresponding damping force F . Choosing appropriate values

for B and G results in the response F being approximately the same as the reference signal, F_R . However, one further modification is required to account for the symmetry of the relationship between applied current and force: when the damping force is negative, increasing the current *decreases* the damping force. This can be compensated for by the modification shown in Figure 5b. To make the device behave as a controllable viscous damper requires the reference force to be proportional to the relative velocity across the damper, as shown in Figure 5c. In this situation the controller gain D can be thought of as the ‘reference damping rate’.

In [14] this control strategy was implemented on a large scale experimental ER damper and it was shown to be effective in enabling controllable viscous damping. However, it was also found [15] that under certain control conditions the experimentally observed response oscillated at high frequency in an undesirable fashion. In the present study this behaviour has been reproduced for the MR damper (Figure 2a and b). The aim of the present article is to explain this behaviour from a control perspective, and to gain further insight from an analysis of numerical simulations and experimental results from the MR damper.

Linear stability analysis

Physical insight into the closed loop-behaviour of the MR damper can be gained by considering a linear representation of the model. At a given instant in time, the contribution of the damping element in Figure 3 can be considered in two parts: a viscous damper c_{lin} representing the behaviour of the device that is not excited by the applied current, and an applied force $F_{lin}=IK_y$ that represents the behaviour due to the applied current. Mathematically,

$$\begin{aligned} c_{lin} &= \left. \frac{\partial \chi}{\partial \dot{x}_2} \right|_{\dot{x}_2, I} \\ K_y &= \left. \frac{\partial \chi}{\partial I} \right|_{\dot{x}_2, I} \end{aligned} \quad (3)$$

The values for c_{lin} and K_y vary depending upon the operating point (\dot{x}_2, I) at which the function χ is linearised. The resulting lumped parameter system is shown schematically in Figure 6a. At one instant in time, the disturbance input x_2 is also fixed, leading to the lumped parameter representation shown in Figure 6b. This linear system can be seen in block diagram form in Figure 6c, where feedback control has been applied. The characteristic equation for this block diagram is:

$$1 + \frac{BGK_y k}{(\tau s + 1)(m_1 s^2 + c_{lin} s + k)} = 0 \quad (4)$$

Rearranging in polynomial form gives:

$$s^3 m_1 \tau + s^2 (m_1 + \tau c_{lin}) + s(k\tau + c_{lin}) + k(1 + GBK_y) = 0 \quad (5)$$

Application of the Routh stability criterion [27] yields the constraint:

$$(m_1 + \tau c_{lin})(k\tau + c_{lin}) > m_1 \tau k(1 + GBK_y) \quad (6)$$

Along with the (intuitive) constraint that the polynomial coefficients in (5) are all positive. Rearranging (6) gives:

$$\frac{c_{lin}^2}{km_1} + \frac{c_{lin}}{k\tau} + \frac{c_{lin}\tau}{m_1} > GBK_y \quad (7)$$

Which suggests that the damper can become unstable for high values of controller gain, B and G . However, the damper can only dissipate energy, and so the system cannot become unstable in the strictest sense. In what follows, the term ‘linear stability’ will be used to represent the behaviour arising due to a violation of (7).

A ‘worst case’ linear stability limit for (7) can be determined by inserting the lowest possible value for c_{lin} , and the highest possible value for K_y . These can be found by a numerical analysis of Equation (1), giving:

$$\frac{871^2}{km_1} + \frac{871}{k\tau} + \frac{871\tau}{m_1} > 2060GB \quad (8)$$

Equation (8) will be used later on in the present study, to compare the linear analysis with experimentally observed behaviour.

This linear analysis offers some physical insight into the behaviour of the smart damper under feedback control, i.e. the influence of the controller gains on the linear stability. However, it does not formally demonstrate limit cycle behaviour of the device, and it requires values for two variables (c_{lin} and K_y) which cannot be readily determined. In the next section, an alternative approach to this control analysis is presented, which seeks to overcome these problems. To begin, the background and nomenclature of nonlinear dynamics is briefly summarised for completeness.

Nonlinear analysis

It is often impossible to find analytical solutions to the equations of motion of nonlinear systems. Consequently the traditional approaches used in control design (such as Laplace transforms and Routh stability analysis) cannot be used directly. However, many simple nonlinear systems can be represented as two dimensional nonlinear ordinary differential equations (ODE's), and in this case a qualitative understanding of the system's behaviour can be gained by studying the phase plane of the system [28].

The phase plane can be used to illustrate the trajectory of the solution of the equations of motion as time progresses. However, it can be more useful to investigate many solutions from different initial conditions as this indicates the so-called 'flow' of the system on the phase plane. Meanwhile, the geometry of the dynamics can be explored by examining the isoclines of the system. These are the loci of points on the phase plane where one of the system equations (ODE's) is equal to zero. Where the isoclines intersect, the time derivative of both states is equal to zero and so the system can be said to be in steady-state. Such points are therefore described as fixed points.

A local stability analysis of the fixed points involves approximating the nonlinear ODE's by corresponding linear equations (using a Taylor expansion), at the operating condition defined by the fixed point. The eigenvalues of the linear ODE's indicate the stability of the fixed point, and the nature of the flow in its vicinity. If the fixed point eigenvalues are complex numbers then the fixed point is termed a focus, as the flow tends to swirl around the focal point. If the eigenvalues have positive real parts then the focus is stable, and flow converges to the fixed point. Stable focal points are therefore analogous to under-damped roots in linear systems. In contrast, unstable fixed points can lead to behaviour such as limit cycles. If the fixed point eigenvalues are real numbers then the fixed point is termed a node; stable nodes being analogous to over-damped roots in linear systems.

For three-dimensional nonlinear ODE's, the same methods can be applied but one must study the phase-space, where the isoclines form planes rather than lines, and the flow is a three dimensional vector field that is difficult to visualise. In what follows, these concepts are applied to the nonlinear model of the closed loop

MR damper. The damper is first described by a set of nonlinear ODE's and the fixed point stability is then determined.

System equations

To begin, the damper is considered in the scenario depicted by Figure 5b. Here, the control input is a constant (F_R) which corresponds to the desired damping force and so the device can be thought of as a semi-active force generator. The closed loop dynamics will be considered for the special case where the mechanical excitation is at constant velocity (ie x_2 is a ramp input). For a damper, one would expect the resulting force to settle to a constant value in this situation.

With reference to Figure 5b, the control current is given by:

$$I_C = G(F_R - BF)\text{sgn}(F) \quad (9)$$

Substituting (9) into (2) yields the closed loop equations of motion for the system:

$$\begin{aligned} \dot{I} &= \frac{G(F_R - BF)\text{sgn}(F) - I}{\tau} \\ m_1 \ddot{x}_1 &= -\mathcal{X}(\dot{x}_1, I) + k(x_2 - x_1) \\ F &= k(x_2 - x_1) \end{aligned} \quad (10)$$

The first step in a nonlinear analysis is to present (10) in ODE form [28]. This can be achieved by defining the following states:

$$\begin{aligned} x_{s1} &= \dot{x}_1 \\ x_{s2} &= x_2 - x_1 \\ x_{s3} &= I \end{aligned} \quad (11)$$

Giving the equations of motion in the nonlinear ODE form:

$$\begin{aligned} \dot{x}'_{s1} &= \frac{1}{m_1} \{-\mathcal{X}(x_{s1}, x_{s3}) + k(x_{s2})\} \\ \dot{x}'_{s2} &= \dot{x}_2 - x_{s1} \\ \dot{x}'_{s3} &= \frac{G(F_R - Bk(x_{s2}))\text{sgn}(k(x_{s2})) - x_{s3}}{\tau} \end{aligned} \quad (12)$$

with the inputs \dot{x}_2 and F_R , and the output $F = k(x_{s2})$. Both of the inputs are now constant values, allowing the phase trajectory to be visualised more easily.

Fixed point stability analysis

The location of the fixed points can be defined by determining the isoclines for each ODE. These are given setting each differential equation in (12) to zero:

$$\begin{aligned} \frac{1}{m_1} \{-\mathcal{X}(x_{s1}, x_{s3}) + k(x_{s2})\} &= 0 \\ \dot{x}_2 - x_{s1} &= 0 \\ \frac{G(F_R - Bk(x_{s2}))\text{sgn}(k(x_{s2})) - x_{s3}}{\tau} &= 0 \end{aligned} \quad (13)$$

The first isocline defines the equilibrium condition between the spring force and the damper force acting on the mass. The second isocline indicates that the relative velocity across the spring is zero, whilst the third isocline is the equilibrium condition for the feedback control.

A fixed point exists where the planes defined by the three isoclines meet. The value of x_{s1} at the fixed point can be readily determined from (13):

$$x_{s1f} = \dot{x}_2 \quad (14)$$

The value of x_{s2} at the fixed point can then be determined numerically by the solution of:

$$k(x_{s2f}) - \mathcal{X}(x_{s1f}, G(F_R - Bk(x_{s2f}))\text{sgn}(k(x_{s2f}))) = 0 \quad (15)$$

Finally, substitution of x_{s1f} and x_{s2f} into (13) leads to the value of x_{s3f} , so that the fixed point is completely defined in phase-space by the three variables x_{s1f} , x_{s2f} , x_{s3f} . The stability of the fixed point can be determined by performing a local linearization of the ODE's at the fixed point, and finding the eigenvalues of the resulting set of linear ODE's.

Local linearisation involves a Taylor expansion of the nonlinear terms in the ODE's (12), neglecting higher order terms, and evaluating at the fixed point. The resulting eigenvalue problem is given by:

$$\begin{vmatrix} -\frac{1}{m_1} \frac{\partial \mathcal{X}}{\partial x_{s1}} \Big|_{x_{s1f}, x_{s3f}} & -\lambda & \frac{k}{m_1} & -\frac{1}{m_1} \frac{\partial \mathcal{X}}{\partial x_{s3}} \Big|_{x_{s1f}, x_{s3f}} \\ -1 & 0 - \lambda & 0 & 0 \\ 0 & -\frac{GBk}{\tau} & -\frac{1}{\tau} - \lambda & 0 \end{vmatrix} = 0 \quad (16)$$

where λ are the eigenvalues of the fixed point. The solution of (16) leads to the characteristic polynomial which dictates the stability of the fixed point. Applying the Routh method then gives the stability constraint:

$$\frac{\left(\left.\frac{\partial\chi}{\partial x_{s1}}\right|_{x_{s1f},x_{s3f}}\right)^2}{m_1} + \left(\left.\frac{\partial\chi}{\partial x_{s1}}\right|_{x_{s1f},x_{s3f}}\right)\left(\frac{\tau k}{m_1} + \frac{1}{\tau}\right) > GBk\left(\left.\frac{\partial\chi}{\partial x_{s3}}\right|_{x_{s1f},x_{s3f}}\right) \quad (17)$$

which defines the stability of the fixed point. It should be noted that (17) is identical to the result obtained from a linear stability analysis (equation (7)), except that the linearised parameters (the partial derivatives) are now known exactly.

Numerical study

The nonlinear analysis described above will now be illustrated by comparing its predictions with those from a numerical simulation.

To investigate the nonlinear dynamics of the MR damper under closed loop control, a time domain simulation of Equation (12) was performed, and the results compared to the nonlinear stability analysis. To begin, the inputs to the control system (\dot{x}_2 and F_R in (12)) were held constant. Next, the effect of digital sampling was investigated. Finally, the input \dot{x}_2 was varied, and F_R made proportional to \dot{x}_2 so as to achieve controllable viscous damping.

Constant velocity, constant reference force

When the inputs to equation (12) are constant values, then the fixed point is at a constant position in phase-space. Consequently the phase trajectory of the system can serve to illustrate the nonlinear dynamics, such as any limit cycle behaviour. The trajectory can also be compared to the fixed-point and isocline geometry. A simulation was therefore carried out using Simulink [29] to solve equation (12) numerically. The initial conditions for all the states was zero, the reference force was $F_R=500\text{N}$, and the mechanical excitation velocity was $\dot{x}_2=0.05\text{ms}^{-1}$. The damper model parameters are shown in Table 1, and the simulation was performed for one value of controller gain G (0.015), and three different values of B (0.3, 0.4, 0.5). For each case a corresponding nonlinear analysis was performed (using the methods described above) to determine the

isoclinic planes (13), the corresponding fixed point ((14) and (15)), its eigenvalues (16), and the fixed point stability (17).

The result for $B=0.3$ is shown in Figure 7a. Here, the nonlinear analysis indicates that the fixed point is a stable focus. Consequently it is expected that the flow will spiral around the focus and eventually converge at the focus, representing a steady-state condition. The phase trajectory obtained from a simulation of equation (12) agrees with the nonlinear analysis. The trajectory spirals around the fixed point, intersecting the isoclinic planes as it spirals, and reaching steady state at the fixed point. In Figure 7b, this result is repeated for the case $B=0.4$. The nonlinear analysis indicates that a fixed point eigenvalue is very lightly damped ($\zeta=0.04$) and so one would expect the oscillations of the phase trajectory around the fixed point to be more severe. The simulation agrees well with this analysis. In Figure 7c, the value of the controller gain B is increased to 0.5, and in this case the nonlinear analysis predicts an unstable focus, i.e. a pair of complex conjugate eigenvalues with negative damping. The phase trajectory (from the simulation) no longer converges to the fixed point, but instead enters a limit cycle, orbiting around the fixed point. The unstable eigenvalue has a natural frequency of 463Hz, which indicates the high frequency of the limit cycle oscillations. If the initial conditions for the simulation are changed, then the system still converges to the same limit cycle, as shown by Figure 7d. However, in this case the trajectory spirals outwards from ‘inside’ the limit cycle.

These results clearly demonstrate how changing the controller gains can cause the damper response to exhibit limit cycle behaviour. This has been made possible by expressing a previously validated model of an MR damper in a form appropriate for phase-space analysis. However, the results are based on two simplifications which make it difficult to compare the numerical and analytical predictions with the experimental behaviour.

The first simplification is that experimental testing of the MR damper has relied on digital control, thus introducing a sampling effect into the system. To assess the effect of the digital sampling, the numerical solutions shown in Figure 7a-c were repeated using a Simulink model that included the effect of controller sampling as a zero-order hold operation. It was found that when the sample time was 0.1ms (as used in the experiments), the stable response was indistinguishable from the continuous time response, but the frequency

of the limit cycle oscillations was very slightly affected. Consequently it remains valid to investigate the experimental behaviour using the continuous-time closed loop model.

The second simplification is that in the damper experiments the mechanical excitation was sinusoidal (rather than at constant velocity), and the desired force was proportional to mechanical excitation (for controllable viscous damping). This issue is investigated below.

Controllable viscous damping

In the experiments, the control strategy shown in Figure 5c was used to emulate controllable viscous damping under sinusoidal mechanical excitation. The corresponding model requires Equation (12) to be rewritten with the reference force, F_R , made equal to $D\dot{x}_2$:

$$\begin{aligned} \dot{x}'_{s1} &= \frac{1}{m_1} \{-\mathcal{X}(x_{s1}, x_{s3}) + k(x_{s2})\} \\ \dot{x}'_{s2} &= \dot{x}_2 - x_{s1} \\ \dot{x}'_{s3} &= \frac{G(D\dot{x}_2 - Bk(x_{s2}))\text{sgn}(k(x_{s2})) - x_{s3}}{\tau} \end{aligned} \quad (18)$$

where the controller gain D represents the reference damping rate, in Ns/m. Close inspection of (18) reveals that the form of the eigenvalue problem (16) is unchanged but the location of the isoclines and corresponding fixed point will move as a function of \dot{x}_2 . As the fixed point moves, then the linearised parameters in (16) will vary, and so there is the possibility that the fixed point stability will also change.

To study this effect, the fixed point stability analysis was repeated for a series of values of mechanical excitation velocity, with two constant values for D . The result is shown in Figure 8, which shows the locus of fixed points in phase-space. To help visualise the locus, it is plotted as a surface defined by the locus and its projection on to the x_{s1}, x_{s2} plane. As the velocity increases, the fixed point moves from an unstable to a stable condition, representing a supercritical Hopf bifurcation [30]. The location of this bifurcation point is affected by the controller reference damping rate, D .

In the next section, experimental results from the MR damper will be compared to analytical and numerical predictions, in a similar fashion.

Experimental study

The theoretical and numerical analysis presented so far has predicted that the MR damper will exhibit limit cycle behaviour under certain closed loop conditions. To validate these predictions, a large number of experimental tests have been performed. A selection of these results will now be compared to the theoretical and numerical behaviour.

Figure 9a shows the experimental behaviour at 15 Hz with $\pm 2\text{mm}$ excitation amplitude, and controller gains $B=0.3$, $G=0.0015$, $D=4\text{kNs/m}$. Using these values for B and G in the linear stability prediction (Equation (8)) indicates that the system is expected to be stable, with no limit cycle. The experimental response shows a small oscillation about the ideal linearised behaviour and no limit cycle is observed. The oscillations only occur for increasing velocity amplitude. Figure 9b shows the corresponding simulation using the nonlinear ODE model (Equation (12)) which exhibits similar dynamic behaviour. In Figure 9c, the numerical simulation is shown as a phase trajectory along with the nonlinear analytical prediction. The analytical prediction is that the fixed point will remain stable as the velocity increases. The phase trajectory illustrates how the system oscillates near the locus of fixed points in an under-damped fashion, but the mechanical excitation frequency is so high that when these oscillations have died out the response never quite settles to the locus of fixed points.

With the controller gains increased to $B=0.5$ and $G=0.002$, the linear stability analysis indicates that the response will not be stable. However, the experimental behaviour under these conditions (shown in Figure 10a) does not exhibit limit cycle behaviour, and is closely matched the simulated response (Figure 10b). The phase trajectory and fixed point analysis (Figure 10c) indicates that a limit cycle exists at low velocities, but as the velocity increases the fixed point becomes a stable focus. Consequently the phase trajectory oscillates about the locus of fixed points, but as the velocity increases these oscillations decay. Despite the existence of this bifurcation point, the simulated and experimental responses (Figure 10a and b) appear to be very similar to those shown in Figure 9a and b. This indicates that the *onset* of limit cycle behaviour is not clearly observed in the experimental and simulated force-velocity response.

In Figure 11 the controller gains are increased further, to $B=0.8$, $G=0.0025$. In this situation the linear stability analysis predicts unstable behaviour, and the experimental response shows much higher magnitude

oscillations which are clearly undesirable. This behaviour is reproduced well by the numerical simulation. In Figure 11c, the phase trajectory orbits around the locus of fixed points, which are now all unstable. This indicates that once the limit cycle behaviour is established *throughout* the sinusoidal operating range then it is clearly observed in the experimental and simulated force-velocity response.

To summarise the results so far, the linear stability analysis has predicted that increasing the controller gains B and G will destabilise the response of the damper. Corresponding experimental results exhibit oscillatory behaviour similar to limit cycles, and this behaviour is both explained and predicted by the nonlinear stability analysis. This analysis indicates that the system can alternate between stable behaviour and limit cycle behaviour as the damper is mechanically excited. The corresponding numerical simulation matches the experimental behaviour very well, and allows the phase trajectory to be plotted in phase-space. When a Hopf bifurcation is present then the response is partly stable, and partly limit-cycle. This makes it difficult to identify the onset of the limit cycle in the experimental results.

To study the effect of the controller gains in more detail, a broader range of experimental data will be studied and the experimentally observed limit cycle behaviour will be subjectively compared to the linear and nonlinear limit cycle predictions.

Limit cycle behaviour

One way of comparing experimental and predicted behaviour is to perform a matrix of experimental tests for different values of the controller gains B , G , and D , along with different mechanical excitation conditions. In Figure 12, some of this experimental data is represented as force velocity responses which have been scaled to fit the graph of B and G . This format enables a subjective visualisation of the effect of B and G on the damper's response. It can be seen that the damping rate increases as G is increased and B is reduced, and that limit cycle behaviour occurs for high values of B and G .

The linear analytical limit cycle predictions can be readily plotted on Figure 12 (using Equation (8)) as a curve of values for B and G that define the stability limit. The nonlinear limit cycle prediction is more complex to determine and requires a numerical method: For a given value of B , the highest value of G is found where the fixed points never have positive damping. This corresponds to a situation where limit cycle

behaviour will occur throughout the test. This analysis must be repeated not only for different values of B , but also for different values of D and the different operating conditions that define the range of the excitation velocity. The resulting curves are also shown on Figure 12.

In Figure 12a and b, the mechanical excitation frequency is 5Hz with an amplitude of ± 2 mm, and a gain D of 5 and 10kNs/m, respectively. It appears that only the highest values of B and G have caused limit cycle behaviour. The nonlinear analysis predicts this very well for Figure 12b, but less accurately for Figure 12a. The linear analysis substantially under-predicts the onset of the limit cycle.

In Figure 12c and d, the mechanical excitation frequency is increased to 10Hz with amplitude ± 4 mm. The gain D is now 2 and 4kNs/m, respectively. In this case, more of the experiments exhibit limit cycle behaviour, and the nonlinear analysis accurately predicts the limit cycle. A similar result is found in Figure 12e and f, where the mechanical excitation is increased to 15Hz with an amplitude of ± 2 mm.

In some cases, the limit cycle that is predicted by the nonlinear analysis is not observed in the experiments. This tends to occur when the value of the gain B is high, and the value of G is low (e.g. Figure 12c, $B=1$, $G=0.001$). This could be because the size of the limit cycle oscillations is too small to observe, but a more likely explanation is that under these operating conditions the model is less accurate.

Discussion

The experimental results presented above are generally in close agreement with the limit cycle predictions of the model. The numerical simulations are able to predict the onset of the limit cycle and this can be illustrated in phase-space. However, the high frequency oscillations observed experimentally are not mimicked precisely by the nonlinear model. This is not surprising: as with the majority of attempts to model smart damper behaviour, the modelling has focussed on low frequencies (ie up to 20Hz). Meanwhile, the nonlinear analysis has shown that a focal point exists in phase-space, which is either under-damped or negatively damped, and has a natural frequency much higher than 20Hz. At these frequencies, the discretisation of the distributed fluid dynamics into a lumped mass and spring will undoubtedly introduce modelling errors. In addition, the stiffness effect due to fluid compressibility is unlikely to be linear, and fluid excitation dynamics (modelled here as a first order lag term) are likely to play a strong role. Despite these issues, the approach described here is still able to predict and explain the observed closed loop behaviour.

In terms of the practical implementation of the techniques described here, it has been shown that a linear stability analysis is relatively straightforward to apply, and consequently this design tool can serve as a starting point for controller specification. The approach could also be used for more complex controllers that rely on classical feedback control techniques, perhaps including the vibrating structure as part of the feedback system. In comparison, the nonlinear stability analysis is more cumbersome to apply, but in this study it has given useful insight into the nature of the closed loop dynamics of the system. If nonlinear controllers are designed for smart dampers, then the nonlinear stability analysis could still be applied. However, the controller states will introduce additional nonlinear ODE's, making the phase-space more difficult to visualise unless the central manifold theorem [17, 30] is used.

A final issue that is worthy of discussion, is the possibility of smart dampers displaying other forms of nonlinear dynamic behaviour, rather than limit cycles. The results presented here have demonstrated that the damper system has only one fixed point, but since the nonlinear ODE's are three dimensional, chaotic behaviour remains a possibility for higher controller gains [30].

Conclusions

The aim of this study was to investigate the closed loop dynamics of smart fluid dampers. The work has focussed on an MR damper operating under proportional feedback control, but similar methods could be applied to other controller designs. The specific conclusions are as follows:

1. It has been shown that a linear stability analysis of the closed loop damper can provide approximate values for the controller parameters, and indicates that fluid compressibility and inertia play a key role in the controller performance. However, this approach does not serve to explain the dynamic (limit cycle) behaviour.
2. Analysis of the nonlinear dynamics of the closed loop damper has explained the experimental limit cycle behaviour for the first time. It has been shown that under sinusoidal mechanical excitation the fixed point for the system is a focus that moves in phase-space and can alternate from stable to unstable conditions. Consequently the limit cycle is not clearly seen in experimental measurements. Despite this fact, the nonlinear model still predicts the experimental behaviour reasonably well, which further validates the modelling approach.
3. The precise nature of the high frequency limit cycle oscillations that are observed experimentally is not accurately predicted by the model. This has been attributed to the modelling errors that are introduced at these high frequencies.

Finally, a common argument in favour of semi-active damping (in particular smart fluid damping), is that it offers an inherent ‘fail-safe’ solution which cannot become unstable, unlike fully active systems. The results presented here demonstrate that such semi-active systems can still produce potentially undesirable closed loop behaviour, which needs to be considered during controller design by using the techniques described.

Acknowledgements

The author is grateful for the support of DSO National Laboratories, Singapore, the assistance of Messrs David Batterbee and Neil Holmes (who collected the experimental data), and the useful discussions with his colleague Dr Roger Stanway. The author is also grateful for the correspondence from Dr Amit Shukla regarding reference [17].

Nomenclature

B	Controller:	Feedback gain
c_{lin}	Linear model:	Damping coefficient
c_{post}	Nonlinear model:	Model damping coefficient in the post-yield condition
c_{pre}	Nonlinear model:	Damping coefficient in the pre-yield condition
D	Controller:	Reference damping coefficient
F	Nonlinear model:	Damping force (model response)
F_{lin}	Linear model:	Force resulting from an applied current
F_R	Controller:	Reference force
F_y	Nonlinear model:	Yield force
G	Controller:	Feed-forward gain
I	Nonlinear model:	Effective current after accounting for excitation dynamics
I_C	Nonlinear model:	Control current
k	Nonlinear model:	Spring stiffness
K_y	Linear model:	Coefficient relating effective current to force
m_1	Nonlinear model:	Fluid inertia
x_1	Nonlinear model:	Coordinate of mass m_1
\dot{x}_1	Nonlinear model:	Velocity of mass m_1
\ddot{x}_1	Nonlinear model:	Acceleration of mass m_1
x_2	Nonlinear model:	Applied mechanical displacement
\dot{x}_2	Nonlinear model:	Applied mechanical velocity
x_{s1}	Nonlinear ODE model:	System state 1
x_{s2}	Nonlinear ODE model:	System state 2
x_{s3}	Nonlinear ODE model:	System state 3
x'_{s1}	Nonlinear ODE model:	Time derivative of system state 1
x'_{s2}	Nonlinear ODE model:	Time derivative of system state 2
x'_{s3}	Nonlinear ODE model:	Time derivative of system state 3
x_{s1f}	Nonlinear ODE model:	System state 1 at the fixed point
x_{s2f}	Nonlinear ODE model:	System state 2 at the fixed point
x_{s3f}	Nonlinear ODE model:	System state 3 at the fixed point
χ	Nonlinear model:	Damping function
τ	Nonlinear model:	Time constant for fluid excitation system

References

1. Simon, D. and Ahmadian, M., 2001, "Vehicle Evaluation of the Performance of Magneto Rheological Dampers for Heavy Truck Suspensions," *Journal of Vibration and Acoustics*, **123**, pp. 365-375.
2. Yoshida, O. and Dyke, S. J., 2004, "Seismic control of a nonlinear benchmark building using smart dampers," *Journal of Engineering Mechanics*, **130** (4), pp. 386-392.
3. Stanway, R., Sims, N. D., and Johnson, A. R., 2000, "Modelling and control of an MR vibration isolator," *Smart Structures and Materials 2000: Damping and Isolation*, **3989**, T. T. Hyde, ed., SPIE, pp. 184-193.
4. Stanway, R., "Smart fluids - the shock of the new," in *Materials World*. IOM Communications Ltd, London, February 2002, pp. 10-12.
5. Choi, S. B., Cheong, C. C., Jung, J. M., and Choi, Y. T., 1997, "Position control of an ER valve-cylinder system via neural network controller," *Mechatronics*, **7**, pp. 37-52.
6. Morishita, S. and Ura, T., 1993, "ER fluid applications to vibration control devices and an adaptive neural-net controller," *Journal of Intelligent Material Systems and Structures*, **4** (3), pp. 366-372.
7. Sims, N. D., Holmes, N. J., and Stanway, R., 2004, "A unified modelling and model updating procedure for electrorheological and magnetorheological vibration dampers," *Smart Materials and Structures*, **13** (1), pp. 100-121.
8. Nakano, M. and Yonekawa, T., 1997, "Active damper using electrorheological suspension and its application to vibration isolation control," *Noise and Vibration Worldwide*, **28** (8), pp. 21.
9. Choi, S.-B., Y T Choi, Park, D. W., and Lee, H. G. I., 1998, "Robust feedback control of a full-car ER suspension system," *Smart Structures and Materials 1998: Smart Structures and Integrated Systems*, **3329**, M. E. Regelbrugge, ed., SPIE, pp. 439-450.
10. Choi, Y.-T. and Wereley, N. M., 2003, "Vibration control of a landing gear system featuring electrorheological/magnetorheological fluids," *Journal of Aircraft*, **40** (3), pp. 432-439.
11. Kim, C. and Ro, P. I., 1998, "A sliding mode controller for vehicle active suspension systems with non-linearities," *Journal of Automobile Engineering*, **212**, pp. 79-92.
12. Choi, S.-B., Lee, H.-S., and Park, Y.-P., 2002, "H-infinity control performance of a full-vehicle suspension featuring magnetorheological dampers," *Vehicle System Dynamics*, **38** (5), pp. 341-360.
13. Jansen, L. M. and Dyke, S. J., 2000, "Semiactive control strategies for MR dampers: Comparative study," *Journal of Engineering Mechanics*, **126** (8), pp. 795-803.
14. Sims, N. D., Stanway, R., Peel, D. J., Bullough, W. A., and Johnson, A. R., 1999, "Controllable viscous damping: An experimental study of an electrorheological long-stroke damper under proportional feedback control," *Smart Materials and Structures*, **8**, pp. 601-615.
15. Sims, N. D., 2000, "Modelling and control of an electrorheological long-stroke vibration damper," PhD Thesis, Department of Mechanical Engineering, The University of Sheffield.

16. Dyke, S. J., 1999, "Stability and performance of controlled civil engineering structures using MR dampers," *Proceedings of the 1999 Structures Congress 'Structural Engineering in the 21st Century'*, ASME, pp. 870-873.
17. Shukla, A. and VanKuren, M. B., 2004, "Nonlinear dynamics of a magnetorheological-fluid-based active suspension system for a neonatal transport," *Smart Structures and Materials 2004: Passive Damping and Isolation*, **5386**, K.-W. Wang, ed., SPIE, pp. 83-93.
18. Lord Corporation, 2003, "MR Damper RD-1005-3 Product Bulletin," http://literature.lord.com/root/product_bulletins/rheonetic/RD_1005_3_2003_19_1.pdf.
19. Sims, N. D., Peel, D. J., Stanway, R., Johnson, A. R., and Bullough, W. A., 2000, "The ER long-stroke damper: a new modelling technique with experimental validation," *Journal of Sound and Vibration*, **229** (2), pp. 207-227.
20. Kamath, G. M., Hurt, M. K., and Wereley, N. M., 1996, "Analysis and testing of Bingham plastic behavior in semi-active electrorheological fluid dampers," *Smart Materials and Structures*, **5** (5), pp. 576-590.
21. Wereley, N. M., 2003, "Nondimensional analysis of electrorheological and magnetorheological dampers using a Herschel-Bulkley constitutive model," *4th ASME-JSME Fluids Engineering Conference*, **FEDSM2003-45046**, ASME.
22. Bitman, L., Choi, Y.-T., and Wereley, N. M., 2002, "Electrorheological damper analysis using an Eyring-plastic model," *Smart Structures and Materials 2002: Damping and Isolation*, **4697**, G. S. Agnes, ed., SPIE, pp. 324-335.
23. Choi, S. B., Song, H. J., Lee, H. H., Lim, S. C., Kim, J. H., and Choi, H. J., 2003, "Vibration control of a passenger vehicle featuring magnetorheological engine mounts," *International Journal of Vehicle Design*, **33** (1-3), pp. 2-16.
24. Sims, N. D., Stanway, R., and Beck, S. B. M., 1997, "Proportional feedback control of an electro-rheological vibration damper," *Journal of Intelligent Material Systems and Structures*, **8** (5), pp. 426-433.
25. Sims, N. D. and Batterbee, D., 2004, "Skyhook damping with linearised MR dampers," *Smart Structures and Materials : Passive damping and isolation*, **5386**, K.-W. Wang, ed., SPIE, pp. 72-83.
26. West, J. C., 1960, *Analytical Techniques for non-linear control systems*. The English Universities Press Ltd, London.
27. Dorf, R. C. and Bishop, R. H., 2001, *Modern control systems*, 9th ed. Prentice Hall, Upper Saddle River.
28. Kaplan, D. and Glass, L., 1995, *Understanding Nonlinear Dynamics*. Springer-Verlag, New York.
29. Simulink, 2003. The MathWorks, Inc. 25 Prime Park Way, Natick, MA, USA.
30. Hilborn, R. C., 1994, *Chaos and nonlinear dynamics*. Oxford University Press.

c_{pre}	100 kNs/m
c_{post}	$(0.6167 + 3.7383 \tanh(1.3629 I))$ kNs/m
F_y	$(-0.0115 + 1.3063 \tanh(1.1946 I))$ kN
k	13kN/mm
m_1	2kg
τ	0.003 s

Table 1: Model parameter values

Table of figures

Figure 1: Damper test facility	24
Figure 2: Experimental results from the MR damper. 10Hz, ± 4 mm. Closed loop response.....	25
Figure 3: Model format [7].....	26
Figure 4: Model validation.....	27
Figure 5: Control concept.....	28
Figure 6: Linearisation process.....	29
Figure 7: Phase-space analysis for constant velocity. $G=0.015$, $F_R=500$ N, Velocity $\dot{x}_2 = 0.05$ m/s,.....	30
Figure 8: Fixed point stability for increasing velocity amplitude,.....	31
Figure 9: Experimental and simulated response, 15Hz, ± 2 mm, $D=4$ kNs/m, $B=0.3$, $G=0.0015$	32
Figure 10: Experimental and simulated response, 15Hz, ± 2 mm, $D=4$ kNs/m, $B=0.5$, $G=0.002$	33
Figure 11: Experimental and simulated response, 15Hz, ± 2 mm, $D=4$ kNs/m, $B=0.8$, $G=0.0025$	34
Figure 12: Experimental and analytical limit cycle behaviour.....	35

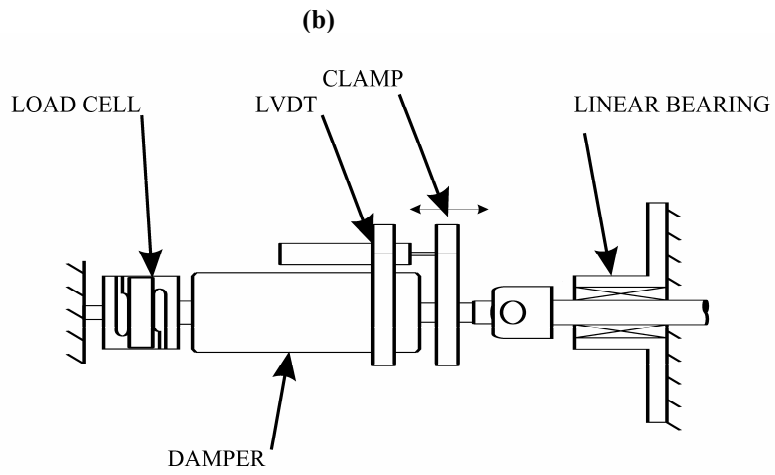
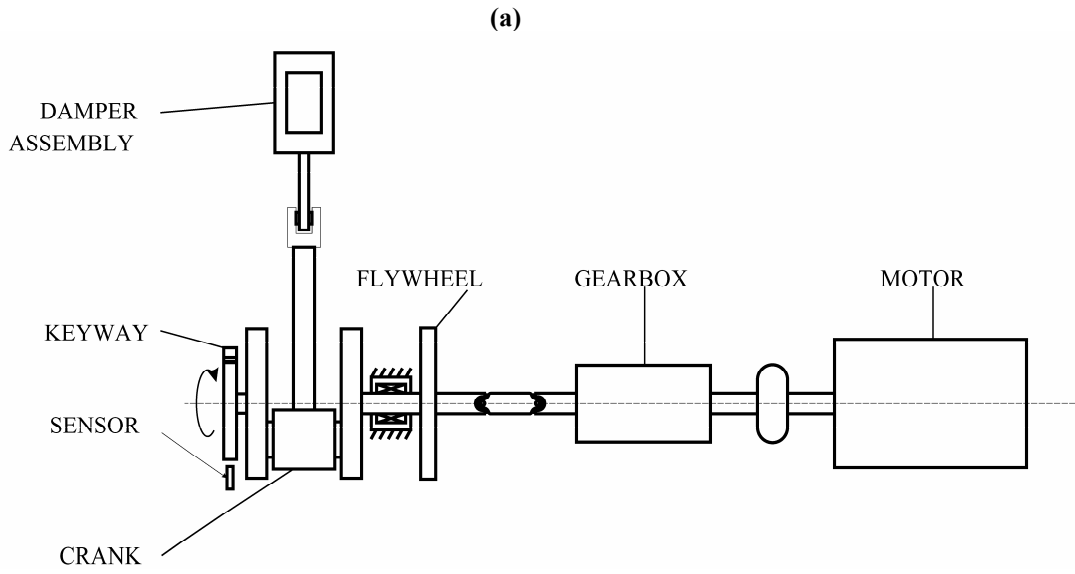


Figure 1: Damper test facility
(a) General configuration (b) Damper attachment

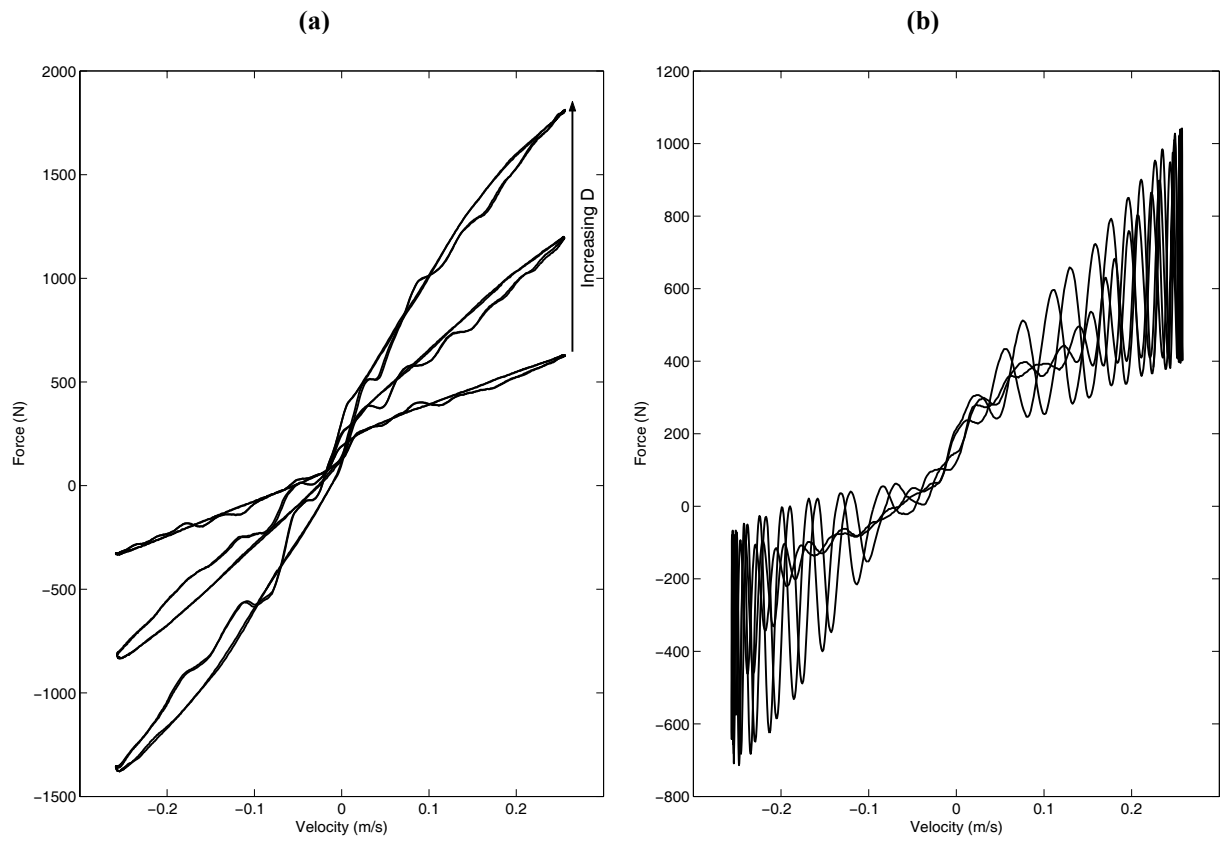


Figure 2: Experimental results from the MR damper. 10Hz, ± 4 mm. Closed loop response.
(a) Controllable viscous damping (b) Increased controller gain causing undesirable closed loop behaviour.

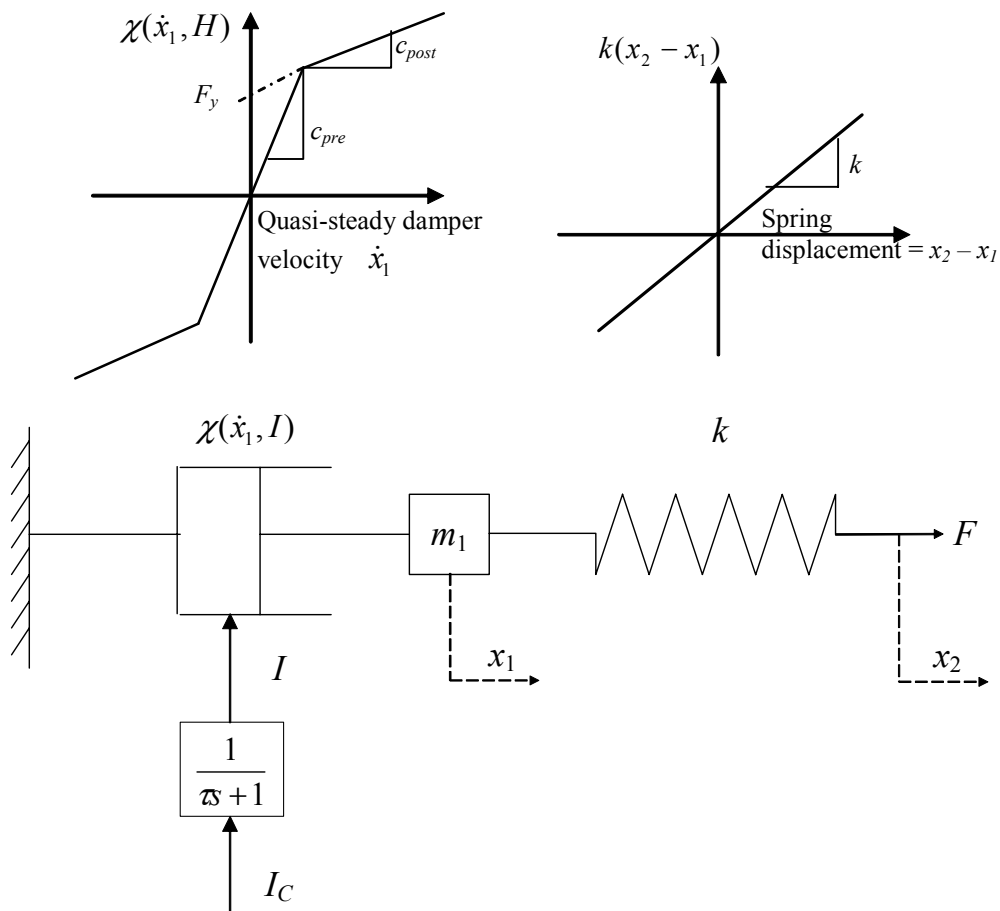


Figure 3: Model format [7].

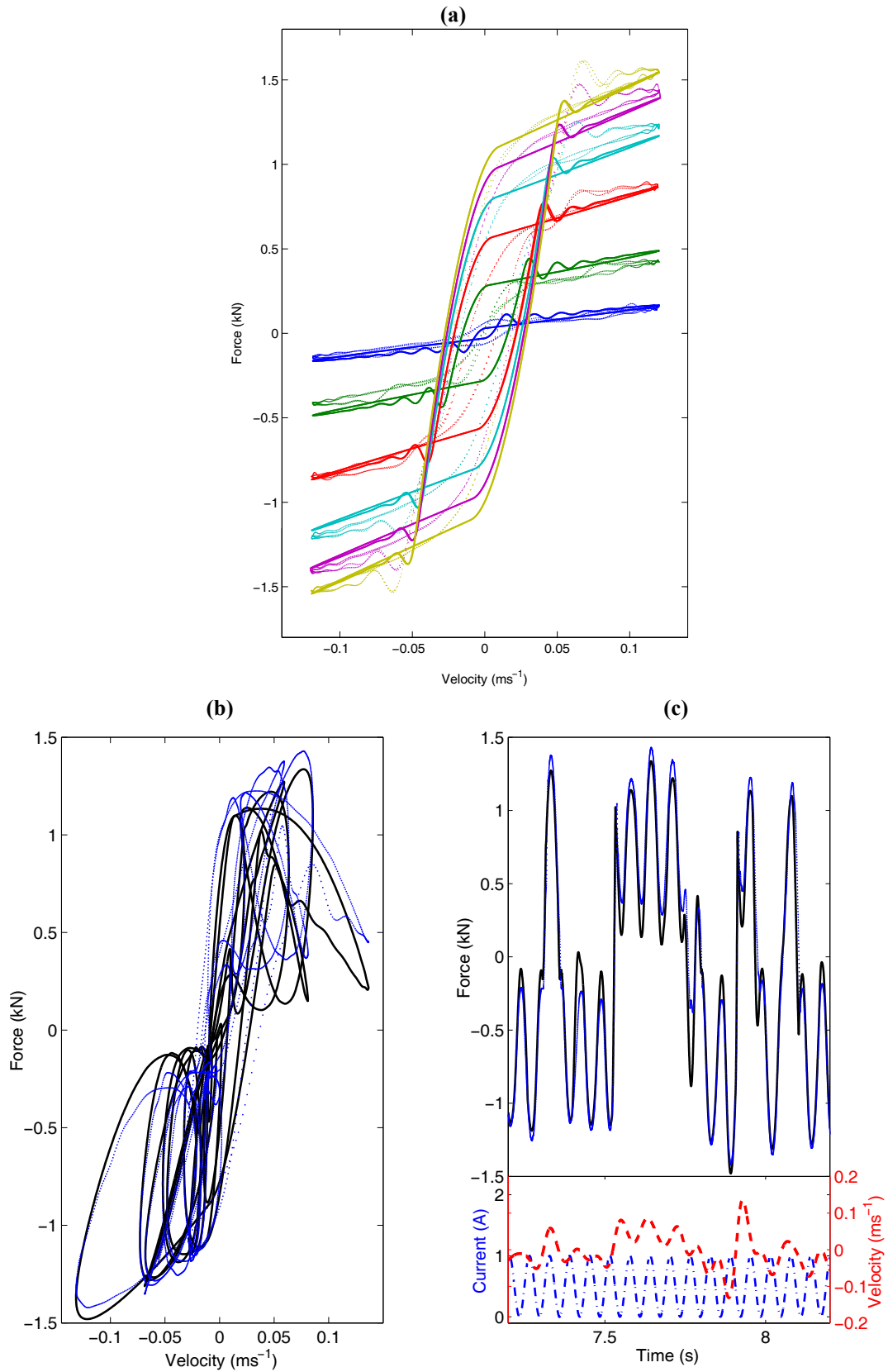


Figure 4: Model validation.

- | | | | |
|---------|------------------|---------|-----------------------|
| ———— | Model response | | Experimental response |
| — · — · | Applied velocity | — · — · | Applied current |
- (a) Sinusoidal mechanical excitation, constant current (0, 0.2, 0.4, 0.6, 0.8, 1.0 A)
 (b) Filtered-random mechanical excitation, sinusoidal input current
 (c) Time history of the result shown in (b).

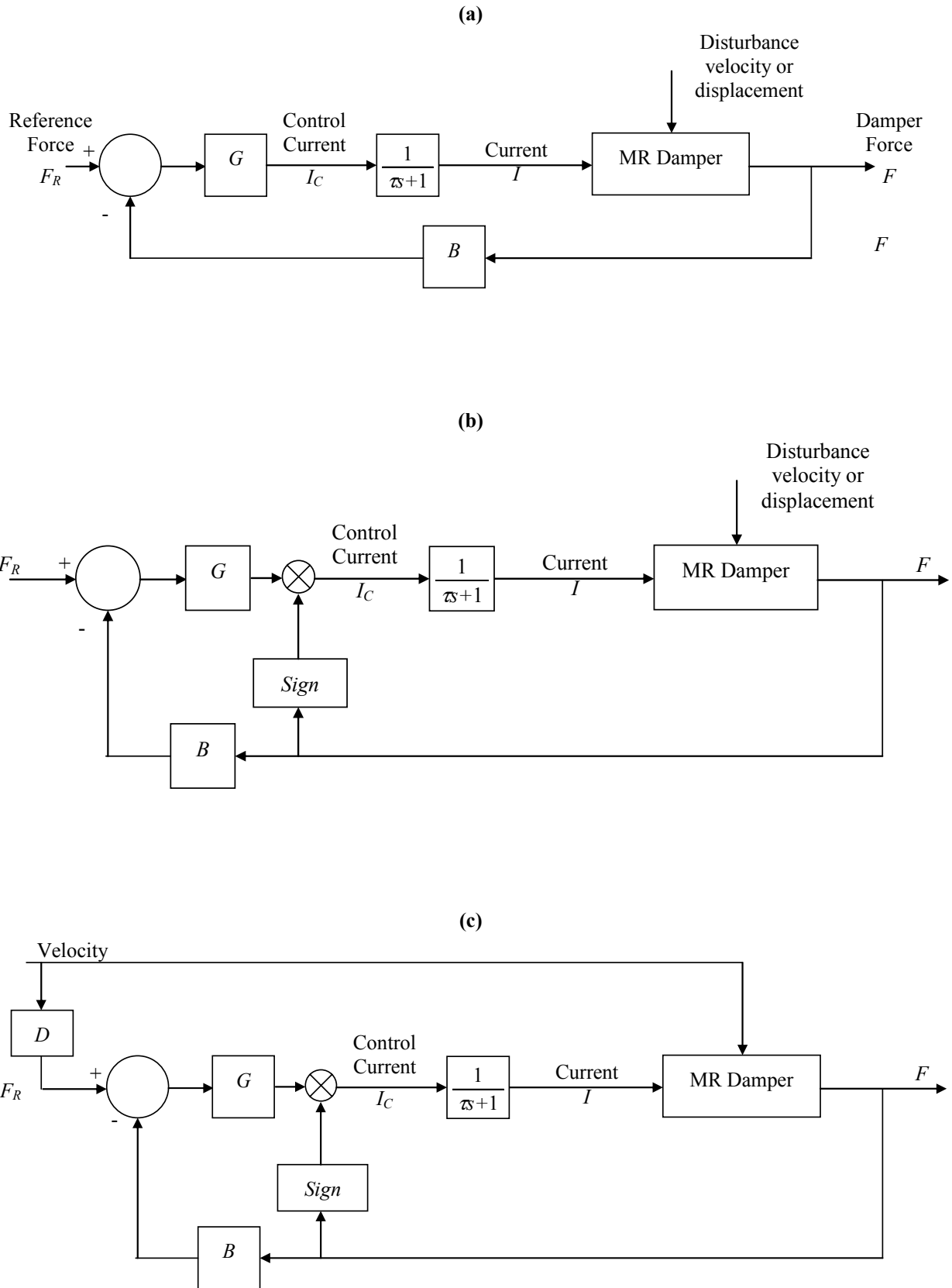


Figure 5: Control concept
(a) basic concept (b) modified to account for symmetry of MR behaviour (c) emulating a controllable viscous damper – the gain D controls the viscous damping rate.

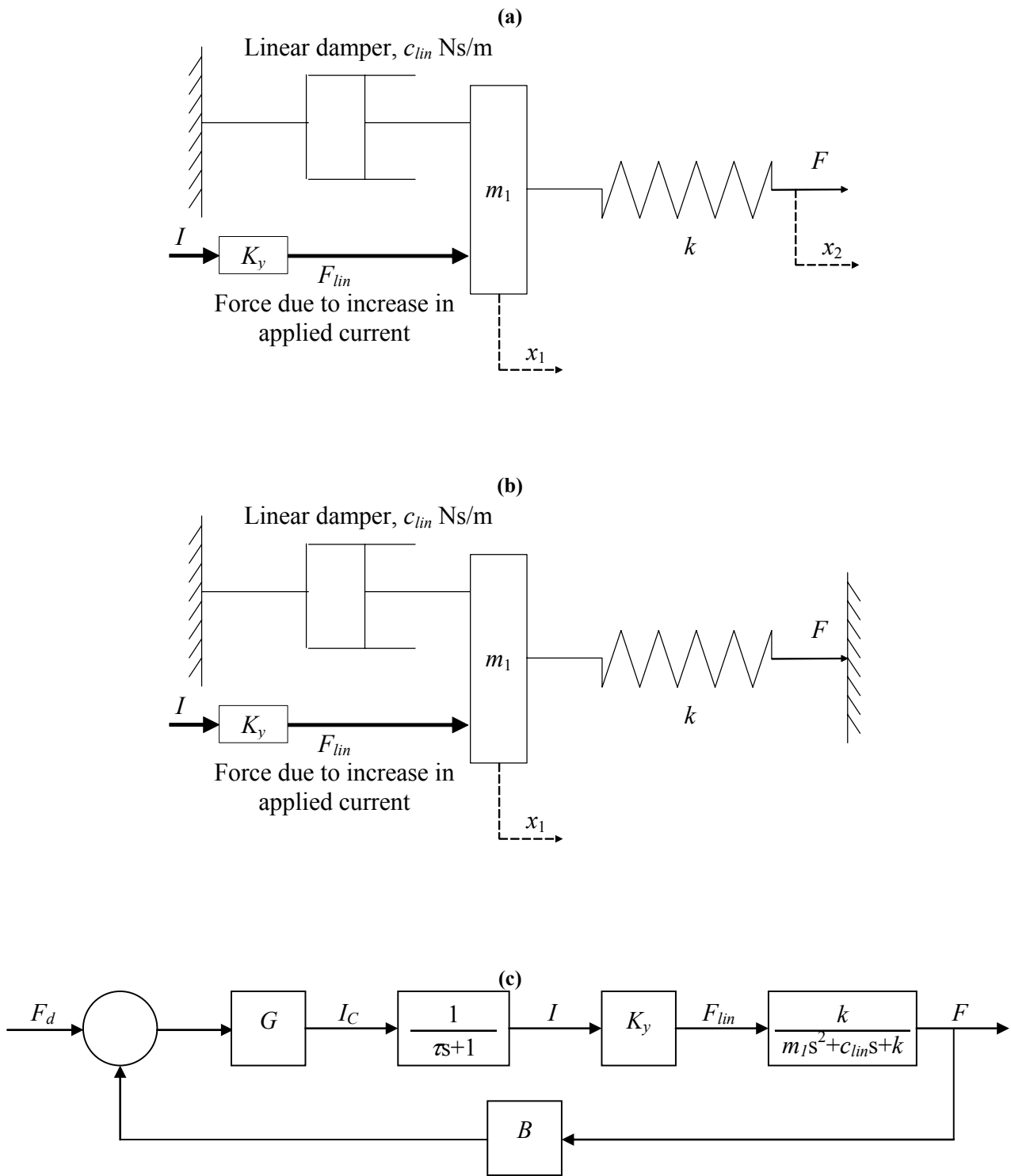


Figure 6: Linearisation process
(a) Linearisation of the model - physical significance
(b) Linearisation about the operating point x_2
(c) Linearised block diagram.

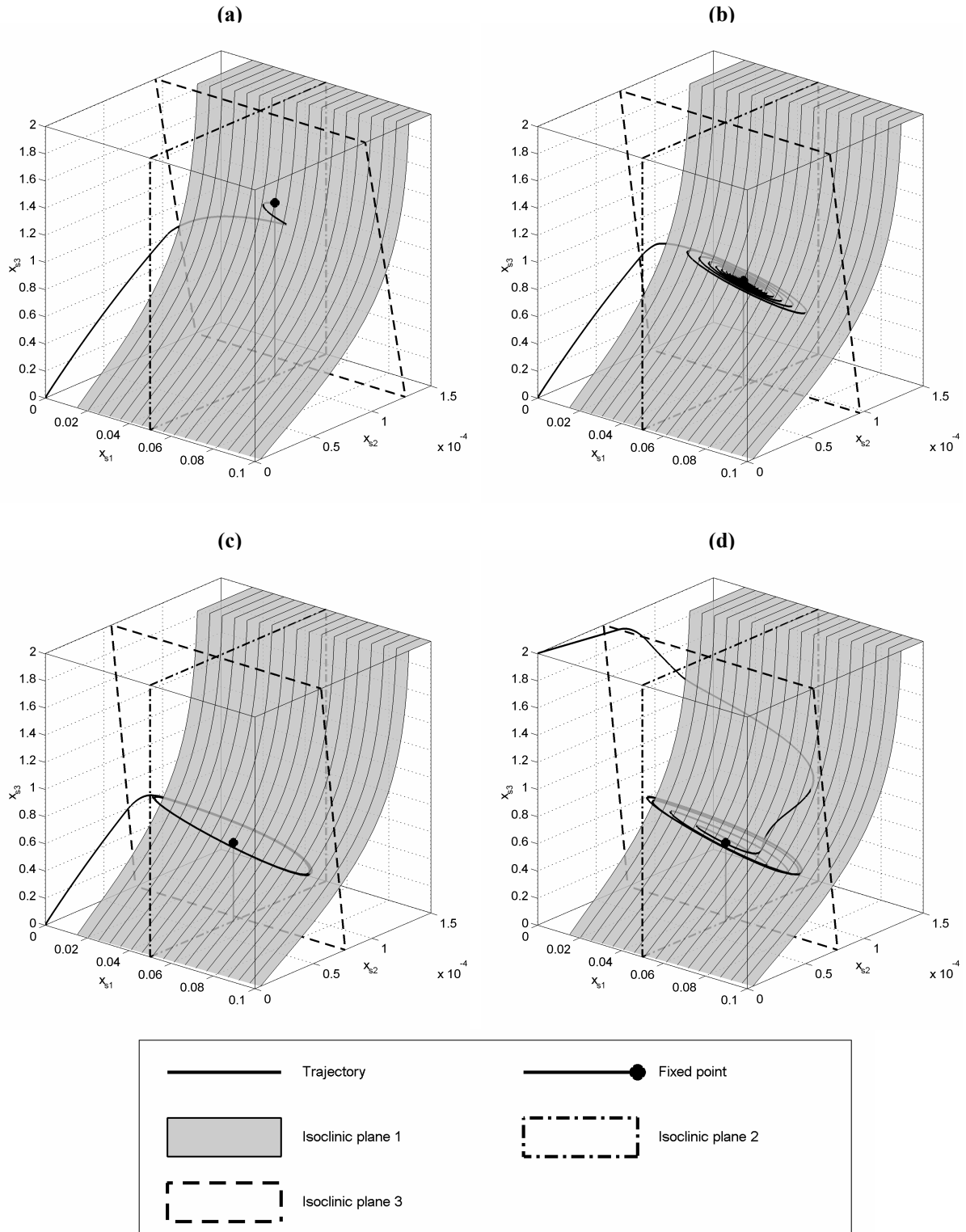


Figure 7: Phase-space analysis for constant velocity. $G=0.015$, $F_R=500\text{N}$, Velocity $\dot{x}_2 = 0.05\text{m/s}$,
(a) $B=0.3$, $\zeta_1=0.3$, $\zeta_2=1$, $\omega_1=2421$ rad/s, $\omega_2=868$ rad/s, stable focus
(b) $B=0.4$, $\zeta_1=0.04$, $\zeta_2=1$, $\omega_1=2593$ rad/s, $\omega_2=1918$ rad/s, stable focus
(c) $B=0.5$, $\zeta_1=-0.1$, $\zeta_2=1$, $\omega_1=2909$ rad/s, $\omega_2=2460$ rad/s, unstable focus
(d) As (c) with different initial conditions.

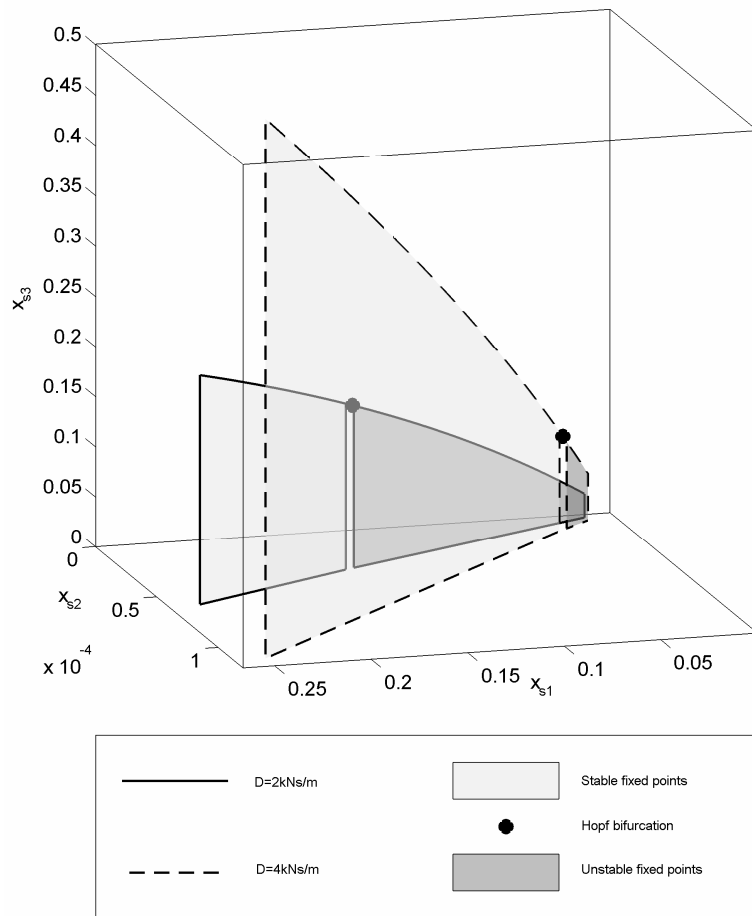
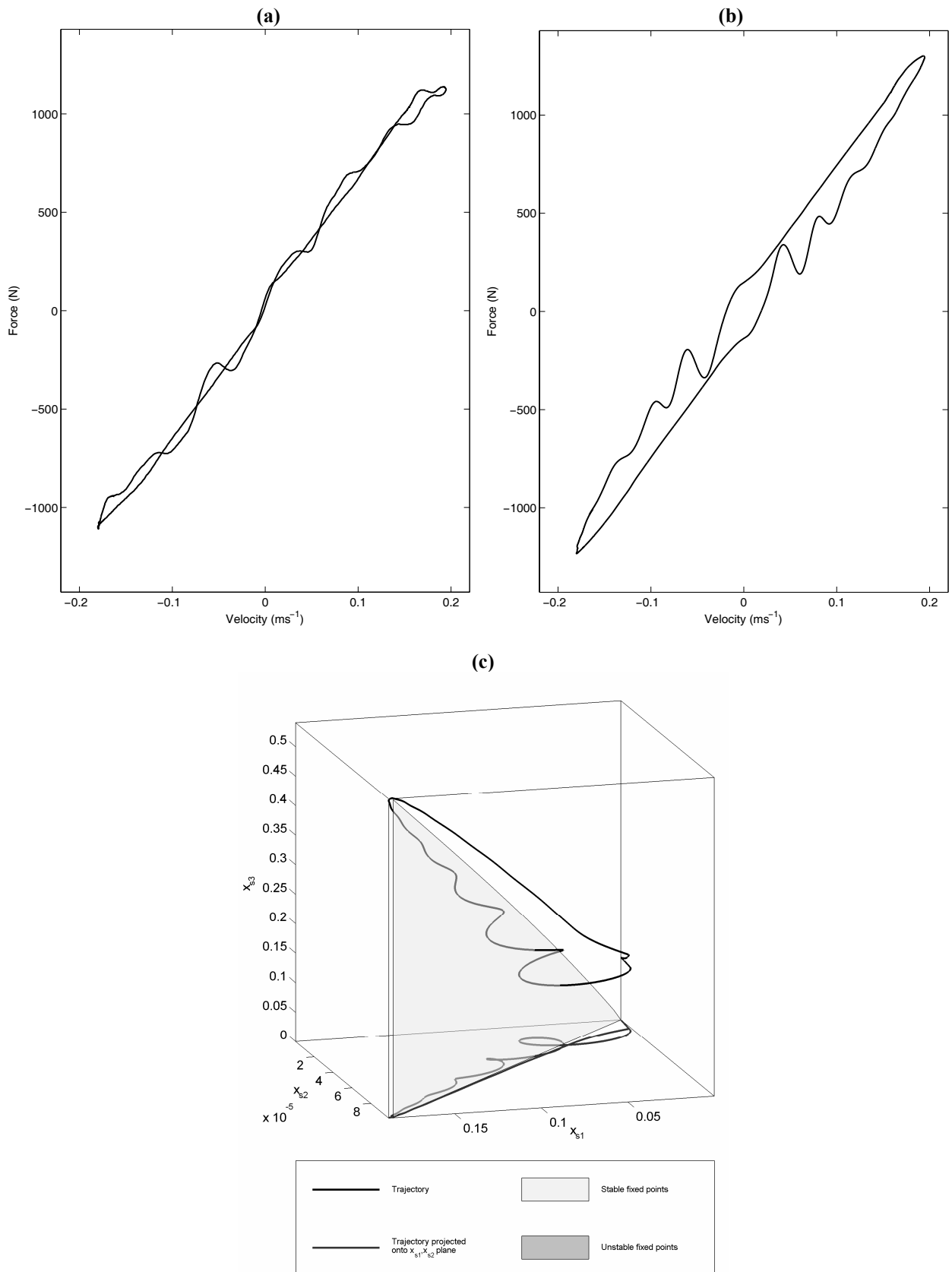
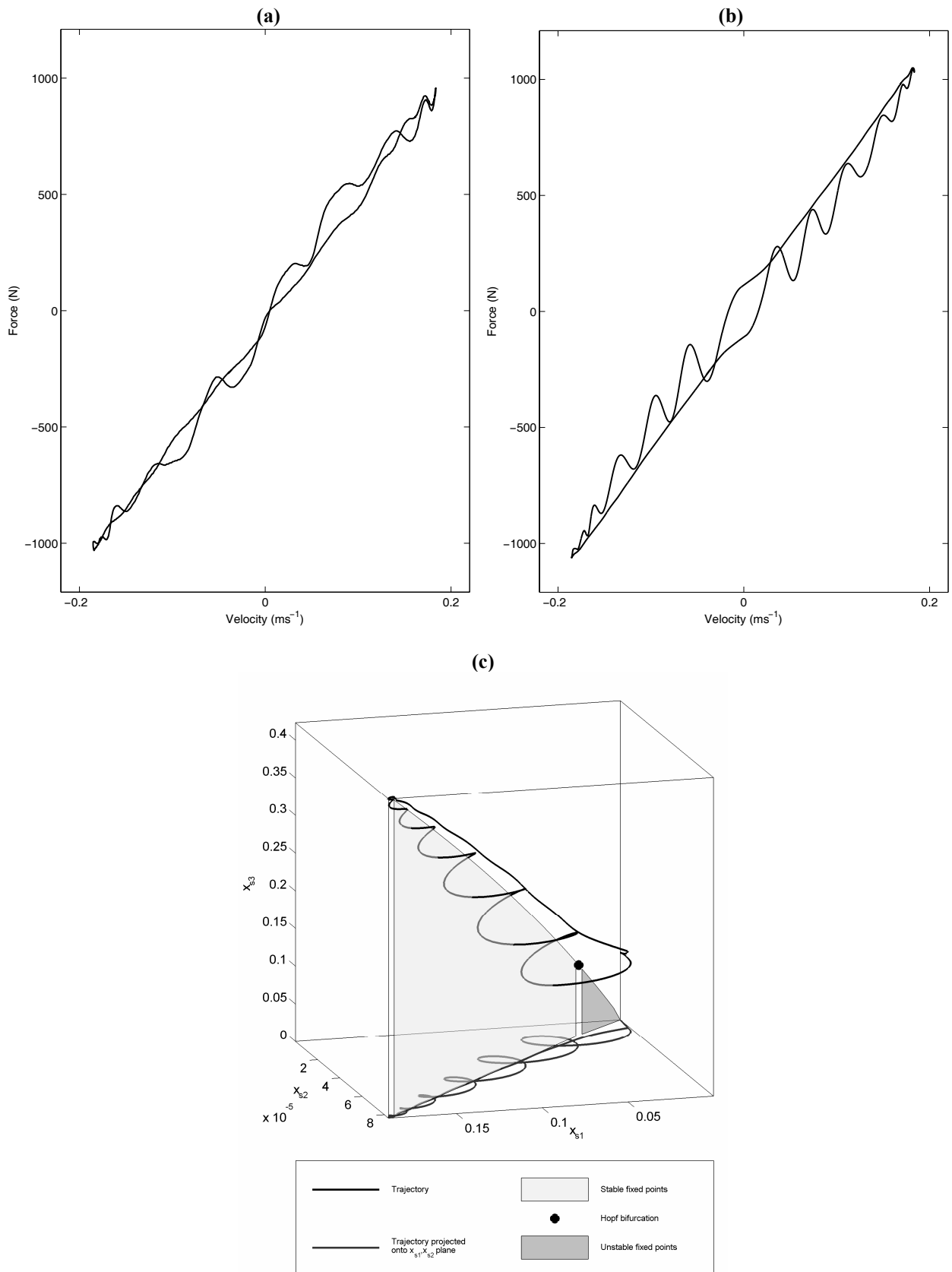


Figure 8: Fixed point stability for increasing velocity amplitude, $B=0.5$, $G=0.002$, $D=2\text{kNs/m}$ and 4kNs/m .



**Figure 9: Experimental and simulated response, 15Hz, $\pm 2\text{mm}$, $D=4\text{kNs/m}$, $B=0.3$, $G=0.0015$.
 (a) Experimental (b) Simulated (c) Simulated phase-space trajectory and fixed points.**



**Figure 10: Experimental and simulated response, 15Hz, $\pm 2\text{mm}$, $D=4\text{kNs/m}$, $B=0.5$, $G=0.002$.
 (a) Experimental (b) Simulated (c) Simulated phase-space trajectory and fixed points.**

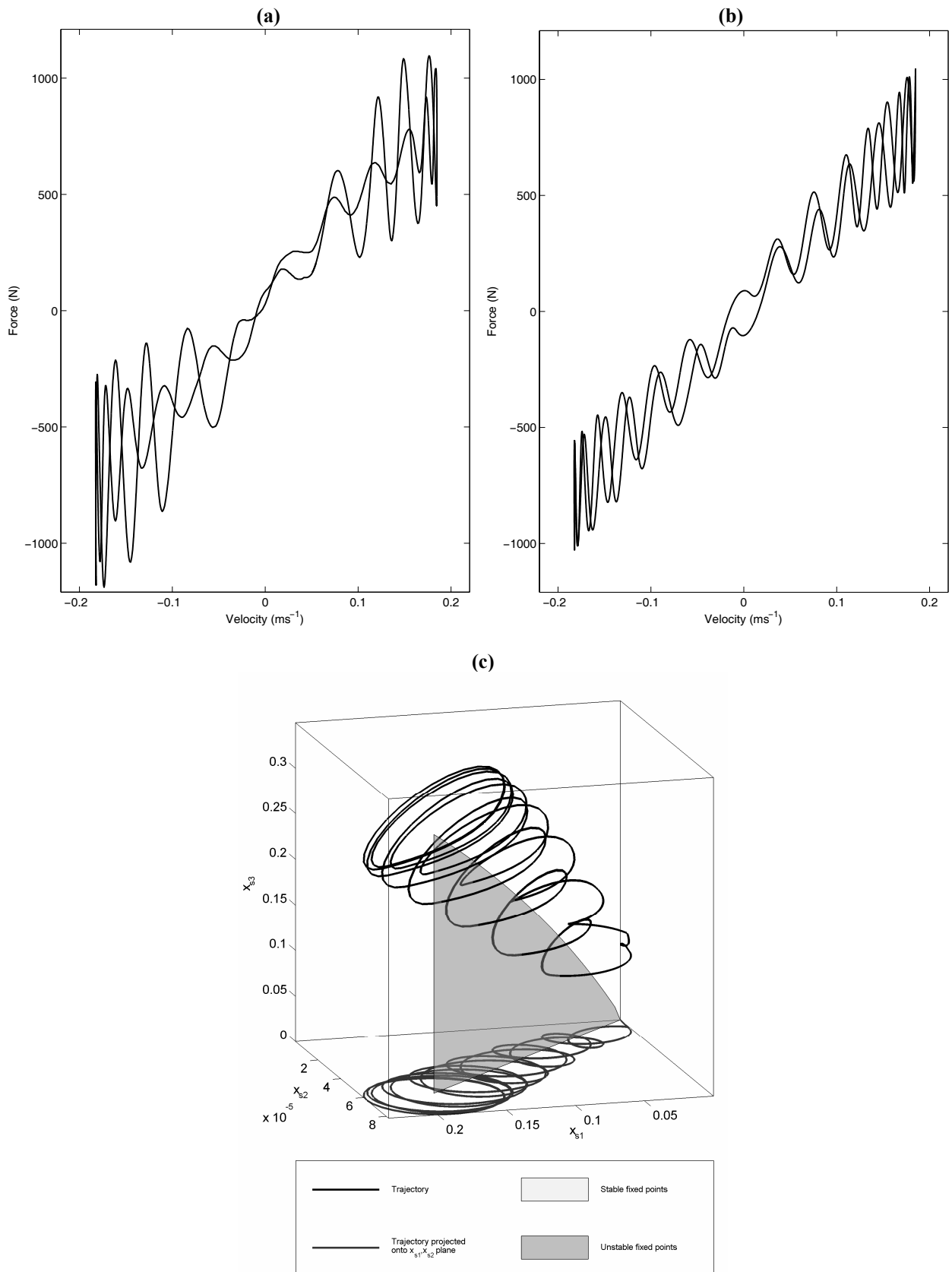


**Figure 11: Experimental and simulated response, 15Hz, ± 2 mm, $D=4$ kNs/m, $B=0.8$, $G=0.0025$.
 (a) Experimental (b) Simulated (c) Simulated phase-space trajectory and fixed points.**

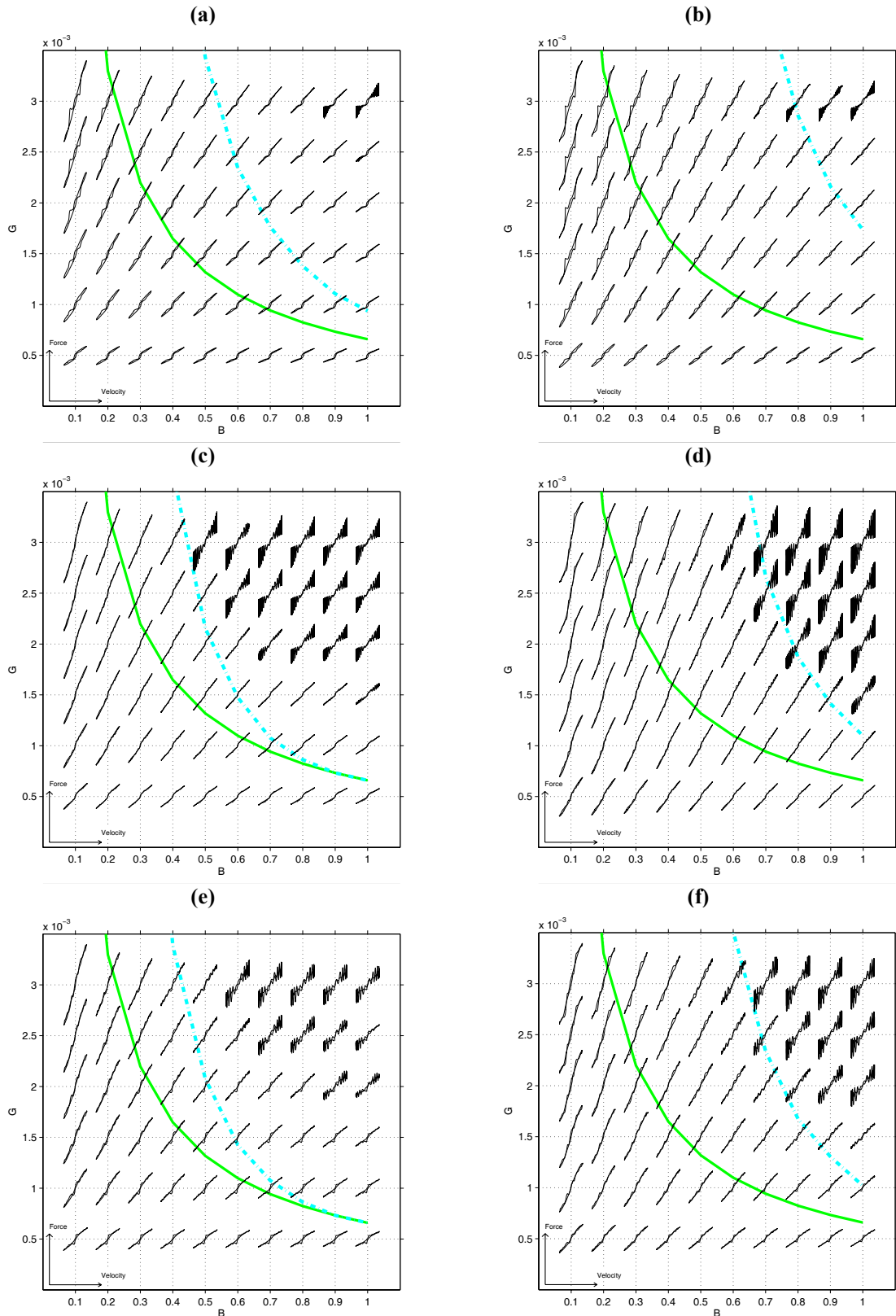


Figure 12: Experimental and analytical limit cycle behaviour.

- Limit cycle: linear analysis
 - - - Limit cycle: nonlinear analysis
 - Experimental force velocity data (scaled)
- (a) 5Hz ±2mm 5kNs/m (b) 5Hz ±2mm 10kNs/m
(c) 10Hz ±4mm 2kNs/m (d) 10Hz ±4mm 4kNs/m
(e) 15Hz ±2mm 2kNs/m (f) 15Hz ±2mm 4kNs/m.